ARL-TR-10030 ● Nov 2024

TiltRotor Aeroelastic Stability Testbed (TRAST) Test and Modeling Data

by Andrew Kreshock, Robert Thornburgh, and Hao Kang

NOTICES

Disclaimers

ARL-TR-10030 ● NOV 2024

TiltRotor Aeroelastic Stability Testbed (TRAST) Test and Modeling Data

Andrew Kreshock, Robert Thornburgh, and Hao Kang
DEVCOM Army Research Laboratory

REPORT DOCUMENTATION PAGE

1. REPORT DATE	2. REPORT TYPE	3. DATES COVERED START DATE	END DATE
November 2024	Technical Report	2 October 2023	25 October 2024

4. TITLE AND SUBTITLE
TiltRotor Aeroelastic Stability Testbed (TRAST) Test and Modeling Data

5a. CONTRACT NUMBER	5b. GRANT NUMBER	5c. PROGRAM ELEMENT NUMBER
5d. PROJECT NUMBER	**5e. TASK NUMBER**	**5f. WORK UNIT NUMBER**

6. AUTHOR(S)
Andrew Kreshock, Robert Thornburgh, and Hao Kang

7. PERFORMING ORGANIZATION NAME(S) AND ADDRESS(ES)	8. PERFORMING ORGANIZATION REPORT NUMBER
DEVCOM Army Research Laboratory ATTN: FCDD-RLA-WF Aberdeen Proving Ground, MD, 21005	ARL-TR-10030

9. SPONSORING/MONITORING AGENCY NAME(S) AND ADDRESS(ES)	10. SPONSOR/MONITOR'S ACRONYM(S)	11. SPONSOR/MONITOR'S REPORT NUMBER(S)

12. DISTRIBUTION/AVAILABILITY STATEMENT
DISTRIBUTION STATEMENT A. Approved for public release: distribution unlimited.

13. SUPPLEMENTARY NOTES

14. ABSTRACT
This report is intended to provide TiltRotor Aeroelastic Stability Testbed (TRAST) model data and test data for understanding the tiltrotor whirl-flutter stability mechanism and for analytical model development and validation. The TRAST model is a semi-span wind tunnel test system designed to test dynamically scaled proprotors in the NASA Langley Research Center Transonic Dynamics Tunnel. The TRAST parameters—including blade flap-pitch couplings (delta-3), pylon pitch spring stiffness, and pylon yaw (diaphragm) stiffness—are adjustable so the effects of control system geometry and wing/pylon dynamics on whirl flutter of the rotors and wings can be investigated experimentally. The TRAST model data includes geometry definition and the structural, inertia, and aerodynamic properties. The test data include ground vibration test data and whirl-flutter stability test data. To support the development of the analytical models for tiltrotor aircraft whirl-flutter analysis, a set of comprehensive analysis models for TRAST whirl-flutter stability predictions are also provided.

15. SUBJECT TERMS
tiltrotor, aeroelastic, stability, whirl flutter, wind tunnel test, modeling and simulation, Weapon Sciences

16. SECURITY CLASSIFICATION OF: a. REPORT	b. ABSTRACT	C. THIS PAGE	17. LIMITATION OF ABSTRACT	18. NUMBER OF PAGES
UNCLASSIFIED	UNCLASSIFIED	UNCLASSIFIED	UU	26

19a. NAME OF RESPONSIBLE PERSON	19b. PHONE NUMBER *(Include area code)*
Andrew Kreshock	757-864-7262

STANDARD FORM 298 (REV. 5/2020)
Prescribed by ANSI Std. Z39.18

Contents

List of Figures v

List of Tables v

1. Introduction 1

2. Background 1

3. TRAST Model Geometry 2

3.1 TRAST 3-D Model 3

3.2 TRAST Mesh Data for 3-D Model 4

4. TRAST Model Properties 5

4.1 NASTRAN Models for Wing and Pylon 5

4.2 Blade Property 6

4.3 Blade Drawings for Section Properties 7

4.4 C81 Table for Blade and Wing Airfoil Aerodynamic Forces 7

4.5 TRAST Control System 8

5. TRAST Experimental Test Date 8

5.1 Ground Vibration Test Data 8

5.2 TRAST Whirl-Flutter Stability Test Date 8

6. RCAS Models for Whirl-Flutter Stability Analysis 15

6.1 Rotor Model 15

6.2 Wing and Pylon Model 15

6.3 Whirl-Flutter Stability Analysis 15

7. Conclusion 16

8. References 17

List of Symbols, Abbreviations, and Acronyms **18**

Distribution List **19**

List of Figures

Figure 1. TRAST in TDT. 3

Figure 2. TRAST wind tunnel test model. 3

Figure 3. Original CAD vs. cleaned CAD. The original CAD involves many small parts that are removed or combined in the cleaned CAD. 4

Figure 4. TRAST assembly mesh. The surface mesh shown is used for CFD analysis on the full TRAST platform. 5

Figure 5. Rotor hub. 7

Figure 6. Example time history. 13

Figure 7. Measured vertical-mode response with various curve fitting trends. . 14

List of Tables

Table 1. List of airfoils and location. 7

Table 2. TRAST test matrix showing pitch-spring stiffness tested for each combination of rotor speed, blade type, and pitch-flap coupling. 9

Table 3. List of rap test runs. 10

Table 4. List of stick-stir test runs. 11

Table 5. List of other miscellaneous test runs. 12

Table 6. List of TRAST digital image correlation tab points. 12

1. Introduction

This report aims to provide the model data, ground vibration test data, and wind tunnel whirl-flutter stability test data of the TiltRotor Aeroelastic Stability Testbed (TRAST). The model data includes the geometry definition and the structural, inertia, and aerodynamic properties. The ground vibration test data includes the measured frequencies for the TRAST components, subsystems, and full model. The wind tunnel test data includes all the test cases of the first and second TRAST stability tests in the NASA Langley Research Center Transonic Dynamics Tunnel (TDT), which is an experimental parametric study of whirl-flutter stability. In addition, this report provides analytical models for TRAST aerodynamics and whirl-flutter stability analyses including the mesh data of the rotor, wing, and pylon, and the comprehensive analysis models for TRAST whirl-flutter stability analysis. This report is intended to provide full sets of data and models for understanding the tiltrotor whirl-flutter stability mechanism, analytical model development, and validation.

2. Background

Aeroelastic stability—specifically whirl-flutter stability—is an important design consideration for any propeller- or proprotor-driven aircraft. The problem of aeroelastic instability was discovered and understood in the 1960s for small, stiff, high-speed propellers typical of fixed-wing transport aircraft. Whirl flutter remains less understood and a significant concern limiting the high-speed performance of large, flexible, more slowly turning proprotors found on tiltrotor and tiltwing aircraft.

A major risk-mitigation step for aeroelastic instability is the use of modeling and simulation analyses to ensure adequate flutter margin. Unfortunately, the data that exist for validation of such tools is largely proprietary and validation of existing analyses has met with limited success. This situation leaves open questions about the validity of the modeling and simulation tools, adequacy of the wind-tunnel models simulating flight hardware, and quality of the experimental data. Without high-quality data and validated analyses to support design efforts, the DoD and U.S. industry must accept a higher level of risk in development than is desirable.

An additional concern is the proliferation of novel large unmanned aerial vehicle (UAV) concepts, some of which are potentially susceptible to aeroelastic instabilities akin to whirl flutter, but not necessarily identical to that predicted for existing aircraft (XV-15, V-22, AW-609). It is unknown whether any existing analysis code can successfully predict stability boundaries for all (or any) proposed winged UAV or vertical takeoff and landing aircraft with large proprotors. Proposed methods of stability augmentation, both active and passive, have barely been addressed. Negligible test data exist for proprotors operating over the extended tip-speed ranges proposed for high-speed tiltrotors.

For over 30 years, the Wing and Rotor Aeroelastic Test System (WRATS) has been used in the TDT to acquire data needed to support research, design, and flight tests of advanced tiltrotors, notably the V-22. Although significantly modified over time, WRATS is limited in the types of rotors it can test and data it can acquire. Its utility for research is further limited by severe restrictions on use and release of design and test data pertaining to the V-22. The aeroelastic phenomena WRATS was intended to explore remain highly relevant, even critical, to the success of future rotorcraft.

Therefore, TRAST is a new test rig that has been developed to fill gaps in experimental data needed to support analysis and design of advanced proprotor aircraft (Kreshock et al. 2019). The TRAST will be used to explore the physics of dynamic coupling between the rotor, airframe, and control system, with focus on proprotor aeroelastic stability (whirl flutter). The TRAST is intended to address the limitations discussed above. It will be operated in the TDT and would accommodate a wider variety of rotors, wings, and control concepts than is now possible.

3. TRAST Model Geometry

The TRAST model is a semi-span wind tunnel test system designed to test dynamically scaled proprotors in the TDT. TRAST can accommodate a gimballed rotor operating at hover and cruise tip speeds typical of tiltrotors or a hingeless rotor operating at very low tip speed during cruise. Powered and unpowered whirl-flutter experimentation can be conducted with the TRAST. TRAST includes a full rotor control system with cyclic and collective controls and wing flaperon controls. The control system is capable of high-frequency inputs for active control studies. Blade flap-pitch couplings (delta-3) are adjustable to explore the effects of control system geometry on whirl flutter of the rotors and wings.

The rotors of TRAST have three blades of 4.0-ft (1.2-m)-radius, Mach-scaled for heavy gas (Figure 1). The development of the TRAST model is described in detail in Kreshock et al. (2019). The TRAST geometry is provided in this section in a format of the 3-D SolidWorks model and Mesh in Computational Research and Engineering Acquisition Tools and Environments’ (CREATE’s) Capstone.

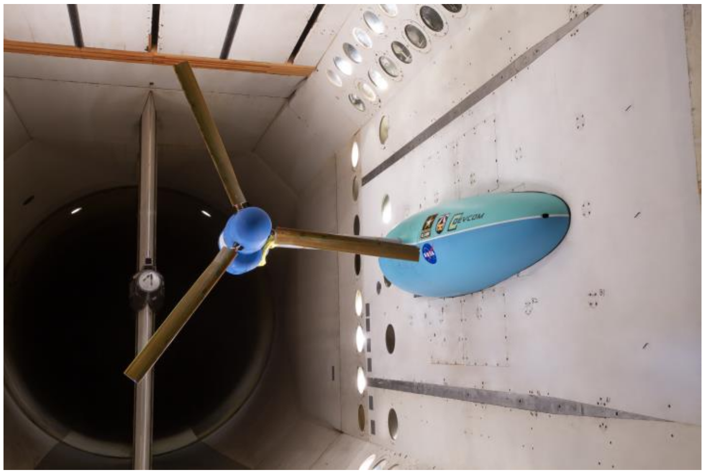

Figure 1. TRAST in TDT.

3.1 TRAST 3-D Model

A 3-D model in a format of SolidWorks or Step is provided for the TRAST geometry (Figure 2). The 3-D model includes all subsystems and parts of the TRAST model and is developed during the critical design of the TRAST.

TRAST 3-D models (including full model assembly, subsystem assembly, and parts) were compressed into a single zipped file in Microsoft Windows with a file name of 2019-08-02-TRAST_Solidworks.zip (2019-08-02 indicates the date that the file was released). To use the model, you need to first extract the file to a desired folder, then open the files in the folder using the SolidWorks software.

Figure 2. TRAST wind tunnel test model.

3.2 TRAST Mesh Data for 3-D Model

A TRAST mesh is also provided for computational fluid dynamics (CFD) analysis. To create the mesh, the original TRAST CAD is first cleaned to remove unnecessary parts and smooth out small features that would make the simulation too computationally expensive (Figure 3). In particular, all nonrotating parts (consisting of the fuselage, wing, nacelle, and hub) are combined into a singular body to eliminate small air gaps between parts that could lead to solution convergence problems from trapped flow. Additionally, each rotor blade is built to be a singular part with a small root cutout to allow for blade motion. The rotor blades are meshed in CREATE's Capstone with 50 spanwise elements and 200 chordwise elements. Elements are clustered in the chordwise direction at the blade leading and trailing edges. At the blade root and tip, 3 times spanwise refinement is applied. The hub and nacelle are meshed with refinement in areas of anticipated stagnation and separation. Lastly, the wing and fuselage are meshed with the CREATE Air Vehicles project's Capstone software, ensuring at least 100 elements along the fuselage length, with 3 times refinement near the wing. To provide sufficient resolution in the blade passage region as well as aft of the wing, a boundary layer is grown off the centerline with first element height equal to 1/30th the fuselage length, 20 layers, and a growth rate of 1.2. The wing is meshed with 50 spanwise elements and 200 chordwise elements, with elements clustered towards the leading and trailing edges. Additionally, 4 times mesh refinement is specified within 3% span of the wing root and tip. The surface meshes for the full TRAST system are shown in Figure 4. Two mesh files are provided for the full TRAST model; the files are TRASTMeshes_body and TRASTMeshes_blade.

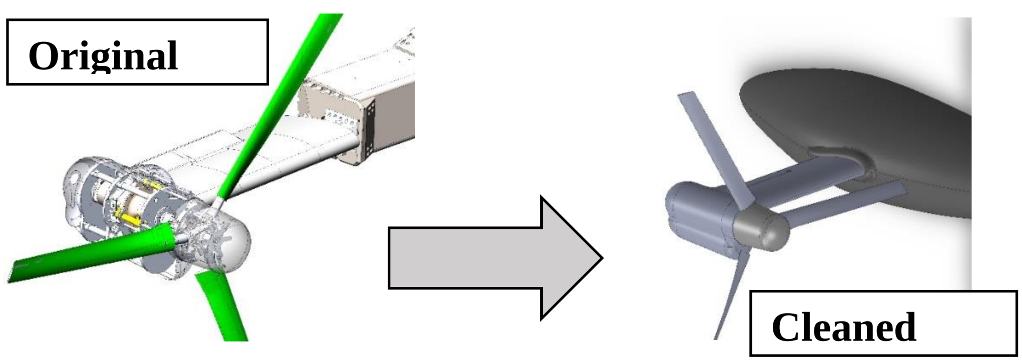

Figure 3. Original CAD vs. cleaned CAD. The original CAD involves many small parts that are removed or combined in the cleaned CAD.

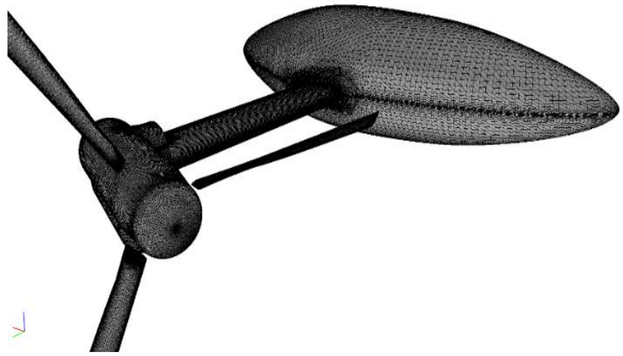

Figure 4. TRAST assembly mesh. The surface mesh shown is used for CFD analysis on the full TRAST platform.

4. TRAST Model Properties

TRAST model properties include the properties of the fixed and rotating systems. The fixed system consists of the wing, pylon, and mast. The fixed system properties are provided in a format of the NASA Structural Analysis (NASTRAN) model. The rotating system includes the rotor system and rotor blade pitch control system. The rotor blade properties are defined in CRUMB—a software generating equivalent property input for both Rotorcraft Comprehensive Analysis System (RCAS) and Comprehensive Analytical Model of Rotorcraft Aerodynamics and Dynamics (CAMRAD).

4.1 NASTRAN Models for Wing and Pylon

There are two finite element models for the wing and pylon structure: a high-fidelity model and a simplified beam representation. The high-fidelity, finite-element model (FEM) of the wing consisted of a shell-element representation of the composite tubular spar connected to 3-D-element representations of the hangers, ribs, and pylon support components. In the simplified model, all components were modeled by beam elements and multi-degree of freedom (DOF) springs.

The composite wing spar was originally modeled by using only the design geometry and material properties, but irregularities in the manufacturing resulted in the need to tune these properties based on empirical data. The properties were adjusted such that they produced excellent agreement with the free-free natural frequencies of the bare spar. After this, all other wing parts were modeled with 3-D elements based on the CAD geometry and connected to the wing-spar model. The bolted connections between the components had to be carefully modeled with limited contact patches so that the assembled model was not too stiff. For the simplified model, the beam properties for the end assembly were chosen to produce an FEM of the wing with similar compliance to the high-fidelity model.

The large stiffness of the wing spar resulted in the predicted compliance and natural frequencies of the wing structure being very sensitive to the modeling of the wing root. The 2.75-in inboard root of the carbon-fiber composite spar is bonded into a stainless-steel spar support flange, which is then bolted using ten 3/8-in socket head cap screws to the spar mount plate. In the high-fidelity model, the spar support flange was modeled with 3-D solid elements and connected to the spar using the permanent-glued contact method. Originally, a rigid constraint was applied to the back side of the spar support flange, but subsequent analysis showed this connection to be excessively stiff. Instead, the spar support flange is constrained only at contact patches for each of the ten socket head cap screws connecting the flange to the mount plate. During subsequent modeling, it was found that the best results were obtained when the ten contact patches were connected to a single wing-root node using an RBE3 constraint element, as opposed to rigidly constraining each of them. This method permits a small amount of relative motion between the bolts during loading and results in a root stiffness that was empirically closer to the TRAST wing. For the simplified model with the beam model for the wing, it was found that the spar support flange had varying degrees of effectiveness at constraining flapwise, chordwise, and torsional loads. Thus, the boundary condition that produced the best correlation with the high-fidelity model was one in which the various DOFs were constrained at different nodes between 2.0 and 2.6 in from the inboard end of the wing spar.

A series of experimental tests was performed to verify that the FEM of the wing assembly accurately represented the TRAST system. The large stiffness of the wing spar made it difficult to accurately measure static-load displacements for model validation, but the natural-frequency measurements produced excellent agreement with the FEMs.

NASTRAN files and notes are collected in TRAST_FEM_v4.zip. A likely starting point is the README.txt and the TRAST2_4k.dat. TRAST2_4k.dat has several options including files for the various TRAST configurations; most of the options are straightforward, with wing_assembly.bdf being the 3-D elements versus wing_beammodel.bdf being beam elements. There are also options such as helicopter versus airplane, control system, hub boundary conditions, and full blades or just a dummy mass. There is also a number convention described in TRAST_numbering.txt that is useful for finding nodes specific nodes.

4.2 Blade Property

The TRAST rotor design is based on the XV-15 rotor. TRAST rotor properties are defined in CRUMB. The original properties were provided by Eagle Aviation

Technologies LLC from the critical design. This data has since been evaluated with Variational Asymptotic Beam Sectional Analysis by the TRAST government team. The file with the blade properties will be in a CRUMB input format that contains the rotor geometric, aerodynamic, and structural properties. The blade root geometry is illustrated in Figure 5.

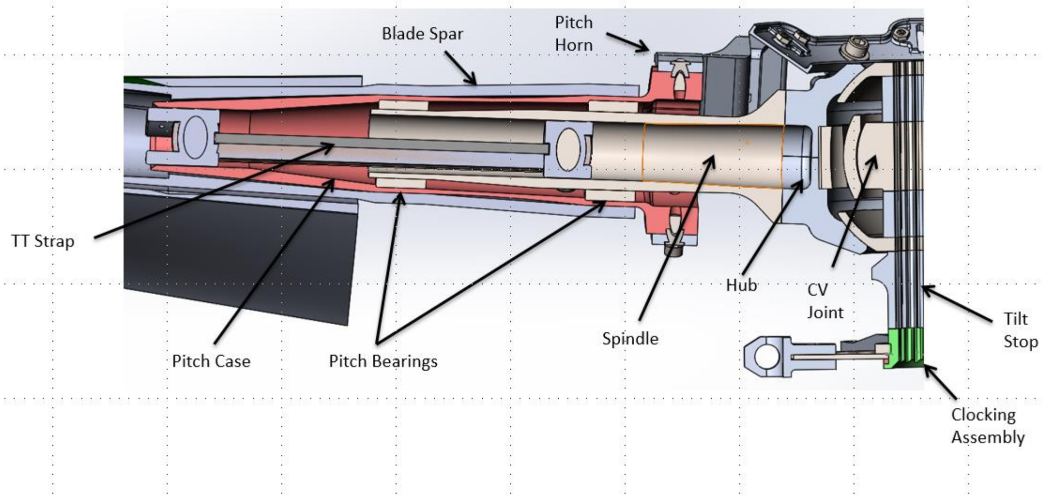

Figure 5. Rotor hub.

4.3 Blade Drawings for Section Properties

The TRAST blade drawings are provided for blade sectional property analysis. The blade sectional property analysis can be used to generate blade properties to validate the properties provided in the NASTRAN model. The results of the analysis can also be used for the comprehensive analysis toolsets.

4.4 C81 Table for Blade and Wing Airfoil Aerodynamic Forces

Blade airfoil tables for five sections are provided in Table 1. These airfoil tables are for the XV-15 because the TRAST rotor blade sections are designed based on the XV-15 rotor.

Table 1. List of airfoils and location.

Airfoil	Location (r/R)
xv15s64x32.c81	0.0
xv1564x25.c81	0.2
xv1564x18.c81	0.55
xv1564x12.c81	0.8
xv1564x08.c81	1.0

4.5 TRAST Control System

Control system geometry and their properties are defined in a standalone spreadsheet called TRAST_Proprotor_DATED.xlsx. The control system geometries are provided for different blade flap-pitch couplings (delta-3) of 0°, 5°, 10°, 15°, 20°, 25°, and 30°. Leading pitch link is positive delta-3 and trailing links are negative delta-3.

5. TRAST Experimental Test Date

TRAST test data includes the ground vibration test data and wind tunnel whirl-flutter test data. The ground vibration test was performed to provide experimental date for structural modeling and validation of TRAST. The whirl-flutter test provided the stability data (frequency and damping) of TRAST and effects of parameters on the stability.

5.1 Ground Vibration Test Data

TRAST ground vibration test data includes frequencies measurements for free-free blade, cantilevered blade, isolated rotor, wing spar, wing spar and driveshaft, wing spar and driveshaft and wing panel, and wing and pylon without rotor as well as with rotor. Detailed information about the measurements can be found in a spreadsheet in Thornburgh and Kreshock (2024).

5.2 TRAST Whirl-Flutter Stability Test Date

The wind-tunnel test was conducted in the TDT with the TRAST mounted to the side wall and operating in airplane mode. All testing was conducted in air (rather than heavy gas) at a nominal tunnel pressure of 1900 psf, except for one configuration where measurements were also obtained at both a higher and lower tunnel pressure to quantify the effect of air density. Stability measurements were performed with the rotor windmilling at the nominal rotor speed (NR) of 909 rpm and at a reduced rotor speed of 727 rpm (0.8 NR). The primary modes that were measured during testing were the wing-vertical mode, which is the low-frequency vertical flapping mode of the wing and pylon that typically goes unstable first, and the wing-inplane mode, which exhibits chordwise wing motion and can result in instability at high tunnel speeds. It should be noted that because of the mass offset of the pylon and the pitch-spring flexibility, these modes include significant amounts of pylon pitch motion as well.

The parametric studies required hardware changes to alter the parameter being investigated and were each treated as a separate configuration. In total, 12 separate configurations were tested, and these are summarized in Table 2. Details of the whirl-flutter tests will be described in Thornburgh et al. (forthcoming).

Table 2. TRAST test matrix showing pitch-spring stiffness tested for each combination of rotor speed, blade type, and pitch-flap coupling.

Pitch-flap	Fiberglass blade			Carbon-fiber blade	
coupling, δ_3	727 rpm	818 rpm	909 rpm	727 rpm	909 rpm
–30°	4k	4k	4k	4k	4k (1700, 1900, and 2100 psf)
–25°	4k	4k	4k	. . .	. . .
–20°	3k, 4k, 5k, 5k*	5k*	3k, 4k, 5k, 5k*	. . .	. . .
–15°	4k	4k	4k	4k	4k
–10°	4k	. . .	4k	. . .	. . .
–0°	4k	. . .	4k	4k	4k

3k: 2862-lb/inch pitch spring, 4k: 4292-lb/in, 5k: 4850-lb/in, 5k*: 4850-lb/inch pitch spring with half-yaw diaphragm spring

The complete set of data from the wind tunnel tests consist of the rap run measurement for each configuration, the stick-stirs run for each configuration and rotor rpm, and other test runs to quantify the model dynamic characteristics with various test conditions and parameters. The rap runs were made before or after the stick-stirs run to measure the model dynamic characteristics for the specific test case. The details of the rap tests are listed in Table 3. The stick-stirs run for each configuration and rotor rpm were made to measure the time response with the stick-stirs and are listed in Table 4. Miscellaneous runs are listed in Table 5 and balance test runs are available in Table 6.

Table 3. List of rap test runs.

Rap test run no.	Configure	Note
Run 1	config_A	No skins installed, no blades, driveshaft disconnected
Run 4	config_A	All skins and aileron installed, no blades, driveshaft disconnected
Run 9	config_A	All skins and aileron installed, no blades, driveshaft disconnected
Run 10	config_A	All skins and aileron installed, with blades, driveshaft disconnected, cold
Run 14	config_A	All skins and aileron installed, with blades, driveshaft disconnected, cold
Run 18	config_A	All skins and aileron installed, with blades, driveshaft disconnected, post-run
Run 21	config_B	All skins and aileron installed, with blades, driveshaft disconnected, cold
Run 26	config_B	All skins and aileron installed, with blades, driveshaft disconnected, post-run
Run 31	config_B	All skins and aileron installed, with blades, driveshaft disconnected, post-run
Run 33	config_C	All skins and aileron installed, with blades, driveshaft disconnected, post-track and balance
Run 39	config_D	All skins and aileron installed, with blades, driveshaft disconnected, post-track and balance
Run 44	config_D	All skins and aileron installed, with blades, driveshaft disconnected, post-run
Run 47	config_D	All skins and aileron installed, with blades, driveshaft disconnected, post-run
Run 49	config_E	All skins and aileron installed, with blades, driveshaft disconnected, post-track and balance
Run 53	config_E	All skins and aileron installed, with blades, driveshaft disconnected, post-run
Run 54	config_F	All skins and aileron installed, with blades, driveshaft disconnected, cold
Run 63	config_F	All skins and aileron installed, with blades, driveshaft disconnected, post-run
Run 65	config_G	All skins and aileron installed, with blades, driveshaft disconnected, post-track and balance
Run 73	config_G	All skins and aileron installed, with blades, driveshaft disconnected, post-run
Run 79	config_H	All skins and aileron installed, with blades, driveshaft disconnected, post-run
Run 81	config_I	All skins and aileron installed, with blades, driveshaft disconnected, post-track and balance
Run 84	config_I	All skins and aileron installed, with blades, driveshaft disconnected, post-run but later
Run 85	config_I	All skins and aileron installed, with blades, driveshaft disconnected, after rubbing check

Table 4. List of stick-stir test runs.

Run type	Run details
Configuration Alpha stick-stirs	Run 12: idle 727 and 909 rpm
	Run 15: flutter clearance 909 rpm
	Run 16: damping measurements 909 rpm
	Run 17: flutter clearance 727 rpm
	Run 19: damping measurements 727 rpm
	Run 20: damping measurements 818 rpm
Configuration Beta stick-stirs	Run 24: flutter clearance 727 rpm
	Run 25: damping measurements 727 rpm
	Run 27: flutter clearance and damping measurements 909 rpm
	Run 30: general predictive control and damping measurements 818 rpm
	Run 101: flutter clearance and damping measurements 909 rpm
	Run 102: damping measurements 909 rpm and some 727 rpm
	Run 104: damping measurements 727 rpm
Configuration Charlie stick-stirs	Run 35: flutter clearance and damping measurements 727 rpm
	Run 36: flutter clearance and damping measurements 909 rpm
	Run 37: general predictive control and damping measurements 818 rpm
Configuration Delta stick-stirs	Run 41: flutter clearance 909 rpm
	Run 42: damping measurements 909 rpm
	Run 43: flutter clearance 727 rpm
	Run 45: flutter clearance 727 rpm
	Run 46: damping measurements 727 rpm, and bonus 909 rpm chord and torsion
Configuration Echo stick-stirs	Run 51: flutter clearance and damping measurements 909 rpm
	Run 52: flutter clearance and damping measurements 727 rpm, plus a few 909 rpm
Configuration Foxtrot stick-stirs	Runs 59 and 60: flutter clearance 909 rpm
	Run 61: flutter clearance and damping measurements 909 rpm
	Run 62: flutter clearance and damping measurements 727 rpm
Configuration Golf stick-stirs	Run 69: flutter clearance and damping measurements 909 rpm
	Run 70: damping measurements 909 rpm, vented
	Run 71: damping measurements 909 rpm, 1700 psf
	Run 72: flutter clearance and damping measurements 727 rpm
Configuration Hotel stick-stirs	Run 76: flutter clearance 909 rpm
	Run 77: damping measurements 909 rpm
	Run 78: flutter clearance and damping measurements 727 rpm
Configuration India stick-stirs	Run 83: flutter clearance 909 rpm
	Run 90: flutter clearance and damping measurements 727 rpm
	Run 92: flutter clearance 818 rpm
	Run 95: damping measurements 909 rpm
	Run 96: damping measurements 818 rpm
Configuration Juliett stick-stirs	Run 110: flutter clearance and damping measurements 909 rpm
	Run 112: flutter clearance and damping measurements 727 rpm
Configuration Kilo stick-stirs	Run 117: flutter clearance and damping measurements 909 rpm
	Run 118: flutter clearance and damping measurements 727 rpm
Configuration Lima stick-stirs	Run 122: flutter clearance and damping measurements 909 rpm
	Run 123: flutter clearance and damping measurements 727 rpm
	Run 124: flutter clearance and damping measurements 818 rpm

Table 5. List of other miscellaneous test runs.

Run type	Run details
No blades	Runs 5 (config A no tape)
	Runs 6–8 (config A with tape)
	Run 127 (config L with tape and spinner holes covered)
Collective sweeps	Run 11
Lag frequency step sine sweeps	Run 27 (config B 727 rpm)
	Run 43 (config D 909 rpm)
	Run 126 (config L 818 rpm)

Table 6. List of TRAST digital image correlation tab points.

Run type	Configuration	Run details
Run 24	91 (1025124235) 92 (1025124316) 99 (1025124911)	. . .
Run 61	F_909	Beam stirs around flutter, plus one chord
Run 69	G_909	Beam stirs around flutter
Run 90	I_727	Beam and chord stirs around flutter
Run 95	I_909	Beam and chord stirs around flutter
Run 102	B_909	Sample yaw, torsion, chord and beam at 60 kts
Run 110	J_909	Sample yaw, torsion, chord and beam at 40 kts
Run 110	J_909	Many beam hits at boundary
Run 112	J_757	Sample yaw, torsion, chord and beam at 40 kts ok, not getting this one
Run 112	J_757	Many beam hits at boundary
Run 117	K_909	Sample yaw, torsion, chord and beam at 50 kts ok, not getting this one
Run 117	K_909	Aileron at 130 kts
Run 117	K_909	Aileron vs. stir at 105 kts
Run 118	K_727	Sample yaw, torsion, chord and beam at 50 kts
Run 118	K_727	Many beam hits at boundary
Run 122	L_909	Positive vs. negative stir for yaw
Run 122	L_909	Aileron vs. stir at boundary
Run 123	L_727	Sample yaw, torsion, chord and beam at 50 kts
Run 123	L_727	Many beam hits at boundary

All test data includes raw data files (i.e., time histories), as shown in Figure 6. The raw time histories include all gages and sensors installed on the model. Gages like strain gages and accelerometers are dynamics sensors and are sampled at 3000 samples/s. Gages like temperature and water flow are not time sensitive and are sampled at roughly 10/s.

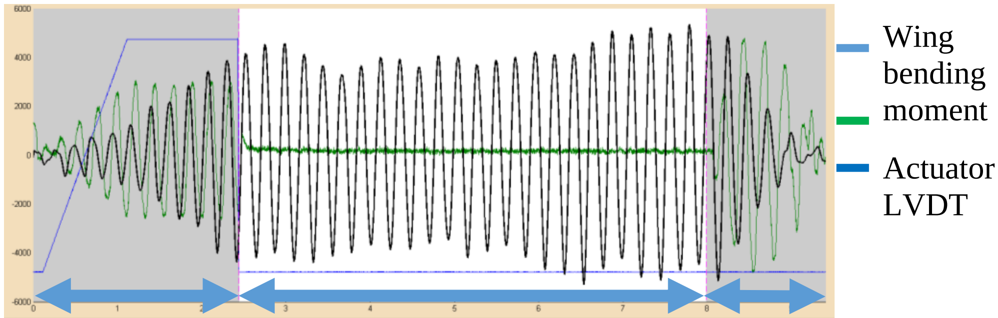

Figure 6. Example time history.

The raw test data is valuable if you are extracting damping and frequency for further use and want to use the raw time histories. Another valuable dataset is the postprocessed data that the rotorcraft aeroelasticity team extracted.

The process of using the free-decay measurements to estimate the system damping is complicated by the wind-tunnel turbulence that induces a quasi-random forced response on the measured system response. Traditional methods for damping estimation from free-decay signals, such as moving-block and Prony techniques, do not account for the presence of a random forced response, and this results in large scatter in their damping estimates. At higher tunnel speeds, the steady-state vibration levels created by the turbulence begin to approach the target amplitudes of the swash plate oscillations. This not only adds a large random response to the free decay, but it also results in fewer cycles before the signal level decays to below the steady-state noise floor. Thus, even averaging the five to ten points per test condition can be insufficient for accurately identifying the system damping at high tunnel speeds. This can be seen in the moving-block damping estimates presented in Figure 7, where the scatter increases with tunnel speed and has a range of around 2% at high speeds.

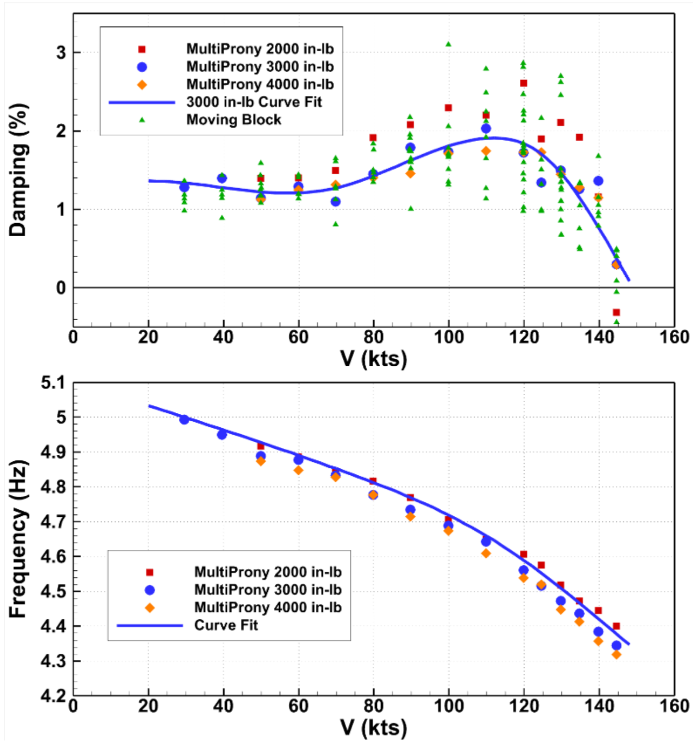

Figure 7. Measured vertical-mode response with various curve fitting trends.

The current measured damping estimates are an attempt to average out the effect of turbulence more effectively. The Prony algorithm is quite effective at extracting frequency and damping from very short segments of a free decay. Over a short enough time segment, the turbulence can be considered as a random impulse on the system. Thus, by using one-cycle segments of time history and incrementing the segment along the time history with 95% overlap, several hundred Prony estimates can be obtained from each free-decay measurement. Averaging these one-cycle Prony estimates from all the decay measurements at a given test condition has resulted in a more consistent estimate for the system damping than simply averaging the small number of moving-block results.

The one-cycle Prony estimates can also be sorted according to the magnitude of the wing bending moment, and then averaged to give frequency and damping as a function of vibration amplitude. As shown in Figure 7, the damping and frequency were often found to vary significantly with vibration amplitude, likely due to the friction in the conversion bearing and hub gimbal. The curve fits that were determined to be a "good fit" for the damping values are based on the 3000-in-lb wing moment levels, since this level had the most available data that was above the steady-state turbulence vibration.

6. RCAS Models for Whirl-Flutter Stability Analysis

Comprehensive analysis models were developed initially to support the TRAST design by using RCAS. The models were then refined gradually based on the real components fabricated, ground vibration test measurements, and whirl-flutter stability test measurements.

6.1 Rotor Model

The rotor blades are modeled based on the TRAST rotor geometry and properties. The blades are highly twisted with a bilinear twist distribution. They have a 2.5° precone, 1° sweep, and constant 4.48-inch chord for the main portion of the blade. Pitch-flap coupling (δ_3) is introduced by the control system geometry. Pitch-flap coupling causes a pitch change when the blade flaps according to the relationship $\Delta\theta = (-tan\delta_3)\beta$, where θ is the pitch angle and β is the flap angle. For the default model, $\delta_3 = 15^{\circ}$. The gimbal is modeled by a constant-velocity joint and the elastic rotor blade was modeled using nonlinear beam elements. Detailed description of the rotor model is given in Kang et al. (2023).

6.2 Wing and Pylon Model

There are two approaches used to model the dynamics of the wing and pylon in the RCAS models. One is to use the nonlinear beam elements and the other is to use the mode shape, modal frequency, and damping from NASTRAN analyses. The nonlinear beam elements model was developed based on the NASTRAN 1-D beam elements model. The RCAS wing/pylon beam element model was developed starting from a spar and more sophisticated models were incrementally built up by adding components one at a time. Natural frequencies are compared with those of the NASTRAN 1-D model at each step. Details of the model development can be found in Yeo et al. (2021).

6.3 Whirl-Flutter Stability Analysis

In the RCAS model analysis, the rotor in airplane mode was first trimmed to zero torque with collective. Then, the stability analysis linearized the equations about the trim solution and calculated frequency and damping using constant-coefficient equations. For both trim and stability analyses, RCAS used no inflow model to calculate induced velocity and quasi-steady (airfoil table look-up) airloads with linear unsteady flow effects based on classical Theodorsen theory. Operating conditions are sea level standard and 909 rpm rotor speed.

The two RCAS model are TRAST_Flutter.rcas, which is the model with NASTRAN modal shape and frequency for the wing and pylon, and TRAST_Flutter_Full.rcas, which is the full RCAS beam element model.

7. Conclusion

This report describes the available test data for the TRAST wind tunnel model. This includes property definitions, higher level model files like RCAS and NASTRAN, and test data that was taken during the latest wind tunnel test (T673). The test data includes multiple configurations and testing techniques and best practices. Ultimately, the hope is this data can be used to improve whirl-flutter predictions for future vertical-lift applications.

8. References

Kang H, Kreshock A, Thornburgh R, Yeo H, Shen J. Correlation of tiltrotor aeroelastic stability wind tunnel test. Paper presented at: Vertical Flight Society's 79th Annual Forum & Technology Display; 2023 May 16–18; West Palm Beach, FL.

Kreshock A, Kang H, Acree W, Yeo H. Development of a new aeroelastic tiltrotor wind tunnel testbed. AIAA Scitech 2019 Forum; 2019 Jan 7–11; San Diego, CA. AIAA; 2019. p. 2019–2133. https://doi.org/10.2514/6.2019-2133

Thornburgh R et al. An experimental parametric study on the whirl-flutter stability of tiltrotors. Paper presented at: Vertical Flight Society's 81st Annual Forum & Technology Display; 2026 May 20–22; Virginia Beach, VA. (forthcoming)

Thornburgh R, Kreshock A. Structural modeling and validation of the TiltRotor Aeroelastic Stability Testbed. AIAA Scitech 2024 Forum; 2024 Jan 8–12; Orlando, FL. AIAA; 2024. p. 2024–1848. https://doi.org/10.2514/6.2024-1848

Yeo H, Kang H, Kreshock A. Modeling and analysis of proprotor whirl flutter. Paper presented at: Vertical Flight Society's 77th Annual Forum & Technology Display; 2021 May 10–14; virtual.

List of Symbols, Abbreviations, and Acronyms

1-/3-D	one-/three-dimensional
CAD	computer-aided design
CAMRAD	Comprehensive Analytical Model of Rotorcraft Aerodynamics and Dynamics
CFD	computational fluid dynamics
config	configure
CREATE	Computational Research and Engineering Acquisition Tools and Environments
CV	constant velocity
DoD	Department of Defense
DOF	degree of freedom
FEM	finite-element model
LVDT	linear variable displacement transducer
NASA	National Aeronautics and Space Administration
NASTRAN	NASA Structural Analysis
NR	nominal rotor speed
RCAS	Rotorcraft Comprehensive Analysis System
TDT	Transonic Dynamics Tunnel
TRAST	TiltRotor Aeroelastic Stability Testbed
TT	tension–torsion
UAV	unmanned aerial vehicle
WRATS	Wing and Rotor Aeroelastic Test System

Nomenclature

θ	blade pitch angle, degree
δ_3	blade flap-pitch coupling
β	blade flap angle, degree

1 DEFENSE TECHNICAL
(PDF) INFORMATION CTR
DTIC OCA

1 DEVCOM ARL
(PDF) FCDD RLB CI
TECH LIB